DOI: 10.6060/ivkkt.20216404.6315

УДК: 544.778.4

ЭЛЕКТРОХИМИЧЕСКИЙ СИНТЕЗ ДИСПЕРСНОГО ФЕРРИТА БАРИЯ С ИСПОЛЬЗОВАНИЕМ АНОДНОГО РАСТВОРЕНИЯ МЕТАЛЛА

И.О. Григорьева, А.Ф. Дресвянников

Ирина Олеговна Григорьева*, Александр Федорович Дресвянников

Кафедра технологии электрохимических производств, Казанский национальный исследовательский технологический университет, ул. К. Маркса, 68, Казань, Российская Федерация, 420015
E-mail: iren-grigor@mail.ru*, a.dresvyannikov@mail.ru

Исследован процесс анодного растворения железа (чистота не менее 99%) в водных растворах хлорида бария, нитрата бария и бинарных электролитах в гальваностатических условиях и методом снятия потенциодинамических поляризационных кривых. Показано влияние состава и концентрации раствора и величины приложенного постоянного тока на интенсивность анодного окисления железа. Выявлено, что скорость окисления металла в бинарных электролитах, содержащих хлорид и нитрат бария, сопоставима с интенсивностью анодного растворения в растворе на основе хлорида бария. Установлено, что анодная поляризационная кривая в растворах, содержащих $BaCl_2$ и $Ba(NO_3)_2$, имеет сложную форму, типичную для пассивирующихся металлов; на ней, как и в растворе нитрата бария, имеет место четкий максимум тока анодного окисления, однако высота пика значительно выше (в 50-150 раз). Предложен способ синтеза дисперсного феррита бария, основанный на анодном окислении железа в водных растворах хлорида и нитрата бария с последующей термообработкой продукта электрохимического растворения. Фазовый и элементный состав и структурные характеристики полученных образцов прекурсора и феррита исследованы с применением рентгенофазового анализа. Показано влияние режима термической обработки на фазовый состав синтезированных образцов. Установлено, что электролиз с растворимым железным анодом при постоянном токе в растворе 0,05М $BaCl_2$ + 0,5М $Ba(NO_3)_2$ и последующая термообработка продукта растворения (1200 °С) обеспечивает формирование дисперсной системы, фазовый состав которой представлен преимущественно $Ba_{0,87}Fe_{11,08}O_{17,15}$ (74%) и $BaFe_2O_4$ (17%).

Ключевые слова: анодное растворение, электролиз, $BaCl_2$, $Ba(NO_3)_2$, железный анод, дисперсная система, феррит бария

ELECTROCHEMICAL SYNTHESIS OF DISPERSED BARIUM FERRITE USING ANODIC DISSOLUTION OF METAL

I.O. Grigoryeva, A.F. Dresvyannikov

Irina O. Grigoryeva*, Alexander F. Dresvyannikov

Department of Technology of Electrochemical Industries, Kazan National Research Technological University, Karl Marx st., 68, Kazan, 420015, Russia
E-mail: iren-grigor@mail.ru *, a.dresvyannikov@mail.ru

The process of anodic dissolution of iron (purity not less than 99%) in aqueous solutions of barium chloride, barium nitrate and binary electrolytes under galvanostatic conditions and by registration of potentiodynamic polarization curves was investigated. The influence of solution composition and concentration and the value of applied direct current on the intensity of anodic oxidation of iron was shown. It was revealed that the oxidation rate of metal in binary electrolytes containing barium chloride and barium nitrate is comparable with the intensity of anodic dissolution in a solution based on barium chloride. It was found that anodic polarization curve in solutions containing $BaCl_2$ and $Ba(NO_3)_2$ has a complex form typical of passivated metals. There is a clear maximum of anodic oxidation current on this curve, as well as in barium nitrate solution, however the peak height is much higher (50-150 times). A method for the synthesis of dispersed barium

ferrite, based on the anodic oxidation of iron in aqueous barium chloride and barium nitrate solutions with subsequent thermal treatment of the product of electrochemical dissolution was suggested. The phase and elemental composition and structural characteristics of obtained precursor and ferrite samples were examined using X-ray phase analysis. The influence of the heat treatment mode on the phase composition of the synthesized samples is shown. It is found that electrolysis with a soluble iron electrode using direct anode current in 0.05M $BaCl_2$ + 0.5M $Ba(NO_3)_2$ solution and subsequent thermal treatment of the dissolution product at 1200 ° C provide the formation of dispersed system, whose phase composition is predominantly $Ba_{0.87}Fe_{11.08}O_{17.15}$ (74%) and $BaFe_2O_4$ (17%).

Key words: anodic dissolution, electrolysis, $BaCl_2$, $Ba(NO_3)_2$, iron anode, dispersed system, barium ferrite

Для цитирования:

Григорьева И.О., Дресвянников А.Ф. Электрохимический синтез дисперсного феррита бария с использованием анодного растворения металла. *Изв. вузов. Химия и хим. технология*. 2021. Т. 64. Вып. 4. С. 59–66

For citation:

Grigoryeva I.O., Dresvyannikov A.F. Electrochemical synthesis of dispersed barium ferrite using anodic dissolution of metal. *Izv. Vyssh. Uchebn. Zaved. Khim. Khim. Tekhnol*. [ChemChemTech]. 2021. V. 64. N 4. P. 59–66

INTRODUCTION

Ferrite-based magnetic materials have a wide range of industrial and technological applications, such as radio and computer engineering, telecommunication, various electronic and electrical equipment devices. Most of the ferrites are ferrimagnets and combine high magnetic susceptibility with semiconductor or dielectric properties, which is why they are broadly used as magnetic materials. Ferrites with a hexagonal crystal structure (M-type) occupy a special place among them, in particular, barium and strontium hexaferrites, which dominate the world market of permanent magnets; they account for more than 90% of the global production of ceramic magnets [1].

At present, M-type hexagonal barium ferrites with the structure of magnetoplumbite $BaFe_{12}O_{19}$ are important magnetic materials [2] and have versatile properties: high values of coercive force, saturation magnetization, magneto-crystalline anisotropy, electrical resistivity, excellent chemical stability, low eddy current loss, relatively low cost, corrosion resistance [3-5].

Such a variety of functional characteristics makes it possible to use barium hexaferrites to obtain new-generation permanent magnets [2], as information carriers with a high recording density [6-7], as absorbing material in various microwave devices and electromagnetic shielding systems [8-9], in medicine, in particular for hyperthermia of malignant cells, treatment of liver cancer, delivery and retention of medicines in the body [7, 10-11].

There are various methods for the synthesis of dispersed powders of hexagonal barium ferrites, in most cases mainly chemical methods are used. The most common and popular methods are chemical coprecipitation [12-13], hydrothermal synthesis [14-15], sol-gel technique [16-17]. Nanosized $BaFe_{12}O_{19}$ has been obtained in the form of ultrafine powders [18], nanocrystals [16], hollow microspheres [19], nanoplates [20], solid [21] and hollow fibers [22]. Traditional methods for producing ferrites are multi-stage processes, characterized by the laboriousness, complexity of the technology and high duration of individual process steps, require high temperatures and high consumption of reagents.

In recent years, a number of electrochemical methods have been proposed [23-26] to be used for obtaining highly dispersed iron-containing oxide systems involving AC and DC electrolysis. For instance, in a study [24] nanodispersed powders of iron oxides were obtained by applying an alternating sinusoidal current to iron electrodes in 17 M NaOH solution. In this case, the maximum powder production rate has been achieved at a current density of 2.5 A/cm^2, a frequency of 20 Hz and an electrolyte temperature of 70 °C. Another study [25] reported on the synthesis of maghemite nanoparticles by electrochemical oxidation of iron electrodes in an aqueous solution of dimethylformamide (DMF) with the addition of cationic surfactants. The electrochemical method for the synthesis of metal oxide powders is the most environmentally friendly and clean. Moreover, such approach allows one to obtain highly dispersed oxide systems and efficiently control the synthesis process and product characteristics (particle sizes, phase and chemical composition) by varying the electrolysis parameters.

The present work focused on the results of a study of the anodic oxidation of Fe in barium chloride and barium nitrate solutions. The objective of this study is to suggest an electrochemical method for producing dispersed ferrites using electrolysis with a soluble anode, as well as to investigate the influence of electrolysis conditions (solution composition and concentration, current density) on the intensity of anodic dissolution of iron and characteristics of the obtained dispersed products.

EXPERIMENTAL PART

Polarization measurements were carried out in a conventional three-electrode electrochemical cell using a platinum auxiliary electrode, commercial Ag/AgCl reference electrode (E = 0.222 V) and working iron electrode under standard conditions (101.3 kPa, 298 K) with natural aeration in the potentiodynamic regime (potential scanning speed of 1 mV/s) by means of a computer-controlled potentiostat-galvanostat model P-301M (Elins). The test iron electrode was of 99.1% purity (elemental composition is given in Table 1) with exposed surface area of 0.36 cm^2. The surface of the test electrode was mechanically polished using diamond paste, degreased with ethanol, and rinsed with double-distilled water before to the experiment.

Table 1

Elemental composition of iron samples (%)
***Таблица 1.* Элементный состав железных образцов (%)**

Fe	C	Si	Mn	P	S	Cr	Mo	Ni	Al	Co	Cu	Ti	V	W
99.1	0.12	0.07	0.45	0.01	0.01	0.01	0.005	0.03	0.005	0.02	0.06	0.002	0.005	0.02

Synthesis of a highly dispersed precipitate was performed via electrolysis in a rectangular cell (80 mm×50 mm×50 mm) of 200 ml using direct current (DC) power supply (MATRIX, model MPS-7101). The plates made of technical iron (99.1% purity) and 12Cr18Ni10Ti stainless steel served as soluble anode and cathode, respectively. The working surface area of the cathode and anode was the same (5 cm^2), the electrodes were located near the opposite walls of the cell, the distance between them was 60 mm. The experiments were carried out at room temperature and natural aeration in aqueous solutions of 0.5 M $BaCl_2$ and $Ba(NO_3)_2$ and binary solutions with different ratio of these components – $BaCl_2$: $Ba(NO_3)_2$ = 1: 1; 1: 2; 1: 3; 1: 4; 1: 5; 1:10. The electrolysis was performed under the following conditions: current density 100-200 mA/cm^2, voltage 8-10 V, electrolysis time 60 min.

For crystallization, the precipitate obtained during electrolysis process was kept in a matrix solution for 48 h; then, it was filtered and dried at a temperature of 80 °C for 2 h. Further, the dried powder was subjected to thermal treatment at a temperature of 1200 °C for 2 h.

X-ray diffraction analysis of the electrolysis and thermal treatment products was carried out by standard technique with a Rigaku SmartLab multifunctional diffractometer using monochromated Cu K_α radiation (λ = 1,5418 Å) operating at 20-60 kV voltage and 2-60 mA current. Phase analysis of the samples was conducted in the step scanning mode (the 2θ scanning step was 0.02°, exposure time at the point was 1 s, the 2θ shooting range varied from 3° to 65°). X-ray diffraction patterns were analyzed using the JCPDS database [27].

A profile analysis of the XRD patterns (phase composition, structural and microstructural parameters of the detected phases) was carried out with PDXL-2 software package. The diffraction peaks were described by the pseudo-Voight function, the background – by B-splines. Due to the fact, that some of the detected phases did not have free access to files containing crystallographic information, the semi-quantitative phase analysis was carried out by fitting the theoretical values of the reflection intensities to the experimental ones and subsequent calculation using corundum coefficients (RIR) in PDXL-2 software package. The refinement of the crystal lattice and microstructure parameters (the size of coherent scattering regions – CSR, the magnitude of microstresses) was performed after a full profile description of the experimental XRD patterns. The calculation of the microstructural parameters was carried out in two ways: the Halder-Wagner method [28] and the method based on the Cagliotti formula [29]. In both cases, the instrumental broadening of diffraction peaks was taken into account, which was determined by shooting a standard sample of silicon powder free of microstresses and dimensional broadening. The lattice parameters and microstructural parameters were refined for phases that had sufficiently intense diffraction maxima.

X-ray fluorescence analysis of the iron anode and obtained precipitate (preliminary investigation) was carried out using a portable X-ray fluorescence spectrometer S1 TITAN (Bruker) with maximum voltage of 50 kV via data packet GeoChem General.

RESULTS AND DISCUSSION

In order to gain an insight into the intensity of anodic dissolution of iron under the DC effect with a maximum yield of its ionization products, we carried out preliminary studies in aqueous solutions of barium chloride and barium nitrate and determined the values of the oxidation rate for iron electrode by the gravimetric method. For the oxidation rate of the metal its weight loss per unit of time (1 h), related to the unit of its working surface, has been taken. According to the obtained data (Table 2), a quite intense dissolution oc-

curs on the surface of iron anode during DC electrolysis in the barium chloride solutions (experiments 1-4, Table 2), which begins along the edges of the plate; the surface of the electrode is covered with a dark brown film, easily washed off with water. The oxidation rate of iron varies slightly with increasing current density from 100 to 200 mA/cm^2 (experiments 1-3, Table 2). On the contrary, an increase in the $BaCl_2$ concentration promotes a more intense dissolution of the metal (experiments 1 and 4, Table 2).

During DC electrolysis in the $BaCl_2$ solution, a suspension of brown, swamp or gray-green color is formed in the electrolyte volume, and dense brown film is formed on its surface. After exposure to the mother liquor (48 hours), filtering and drying for 2 h at 80 °C the powder of brown color is formed. A preliminary X-ray fluorescence analysis revealed the presence of a significant amount of barium, chlorine and a low iron content in the obtained samples (experiments 1-3, Table 2).

During electrolysis in barium nitrate solutions (experiments 5-6, Table 2), the metal oxidation with the subsequent formation of the precipitate in the bulk of the solution does not occur with the weight loss of the iron electrode tending to zero. Since active ionization of iron does not occur, we can assume that in this case there is passivation of the anode surface due to the formation of an oxide film.

Table 2

Oxidation rate of iron in the DC mode

***Таблица 2.* Скорость окисления железа при постоянном токе**

№ п/п	Solution composition	Current density, mA/cm^2	Oxidation rate, (mg/cm^2·h)
1	0.5 M $BaCl_2$	100	164
2	0.5 M $BaCl_2$	150	178
3	0.5 M $BaCl_2$	200	189
4	1.0 M $BaCl_2$	100	225
5	0.5 M $Ba(NO_3)_2$	100	0
6	0.5 M $Ba(NO_3)_2$	150	0
7	0.5 M $BaCl_2$ + 0.5 M $Ba(NO_3)_2$	150	158
8	0.2 M $BaCl_2$ + 0.6 M $Ba(NO_3)_2$	150	145
9	0.1 M $BaCl_2$ + 0.4 M $Ba(NO_3)_2$	150	142
10	0.05 M $BaCl_2$ + 0.25 M $Ba(NO_3)_2$	150	162
11	0.05 M $BaCl_2$ + 0.5 M $Ba(NO_3)_2$	150	166

Fig. 1 presents the anodic potentiodynamic curves (potential-current, E = f(j) curves) of iron in the studied single-component solutions. One can see relatively low values of the corrosion potential in these media: from (-90) - (-115) mV in $BaCl_2$ to (-110) - (-130) mV in $Ba(NO_3)_2$. The presence of chloride ions, which are classical activators of the anode process, as well as an increase in their concentration leads to an increase in current density and the rate of dissolution of iron (Fig. 1a).

A different picture is observed in the barium nitrate solutions (Fig. 1b). The E = f(j) curves have a typical form that is characteristic of passivating metals – an active zone of anodic dissolution (or active-passive transitions) with the presence of current maximum (peak), passivity region and region of oxygen evolution are clearly visible on these dependences. The anodic curve exhibits current peak near 0-30 mV (current values do not exceed 10 mA/cm^2), which should be associated to formation of a passive layer on iron. The current peak reaches its highest values in 0.1 M $Ba(NO_3)_2$ solution; at other concentrations, its value decreases by about half. The extent of the passivity region is 475-600 mV (Fig. 1b).

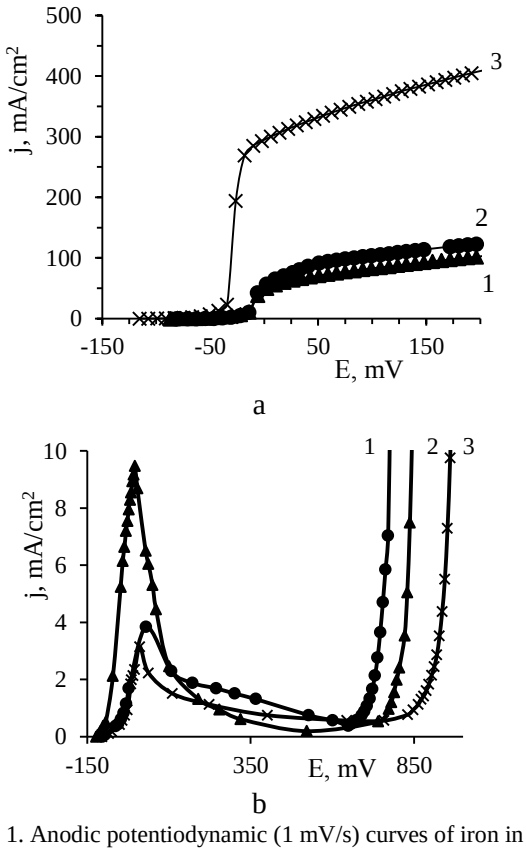

Fig. 1. Anodic potentiodynamic (1 mV/s) curves of iron in (a) $BaCl_2$ and (б) $Ba(NO_3)_2$. Solution concentration, mol/l: 1 – 0.05; 2 – 0.1; 3 – 0.5

Рис. 1. Анодные потенциодинамические (1 мВ/с) кривые железа в $BaCl_2$ (а) и $Ba(NO_3)_2$ (б). Концентрация раствора, моль/л: 1 – 0,05; 2 – 0,1; 3 – 0,5

In order to determine the optimal electrolysis conditions for obtaining the product, two-component solutions, $BaCl_2$ + $Ba(NO_3)_2$, were also investigated. In these media, the anodic polarization curve also has a complex shape typical of passivated metals (Fig. 2a and curve 3 in Fig. 2b). It can be seen a clear current maximum of the anodic oxidation, as well as in the $Ba(NO_3)_2$ solution (Fig. 1b), however, due to activation of the electrode surface by chloride ions, the peak height increases significantly and corresponding current density values are 50-150 times higher than in $Ba(NO_3)_2$. In addition, the oxidation peak becomes much more extended in width (on average in the range from -200 to 1000 mV) and shifted to higher potential. Next, for higher potential values (above 900-1000 mV) a relatively short passivity region (length 350-400 mV) is observed (Fig. 2a).

Further, in order to obtain a product of the required composition and with a maximum yield, electrochemical synthesis of dispersed samples was carried out in binary electrolytes with different contents of barium chloride and barium nitrate, ratio of components is $BaCl_2$: $Ba(NO_3)_2$ = 1:1; 1:3; 1:4; 1:5; 1:10. According to the data (experiments 7-11, Table 2), a change in the ratio of components weakly affects the intensity of the anodic dissolution of iron, the values of the oxidation rate in all cases are comparable. In these media, unlike the $BaCl_2$ solutions, the anodic dissolution of metal, as a rule, starts from the 5-10th min of the process.

The product of DC electrolysis in the 0.05M $BaCl_2$ + 0.5M $Ba(NO_3)_2$ solution is initially a suspension of marsh color. After its holding in the matrix solution for 48 h, a two-layer precipitate is formed with clear layer boundaries: brownish-green lower layer with a height of 10-25 mm (with a cell width of 50 mm), and the upper layer (5-10 mm high) is brown or red-brown in color. This indicates the spatial separation of the oxidation products of metallic iron, which are present in the form of compounds with a predominance of iron (II) in the lower layer of the precipitate, and, conversely, iron (III) – in the upper one. This indicates the spatial separation of the products of oxidation of metallic iron, which are present in the form of compounds with a predominance of iron (II) in the lower layer of the precipitate, and, conversely, iron (III) in the upper one. After precipitate filtering, drying and mechanical grinding at room temperature, a light-brown product is formed. After precipitate drying at 80 °C for 2 h, its color becomes more saturated and changes to dark brown. After thermal treatment of the sample at 1200 °C for 2 h, the color of the product becomes darker, almost black.

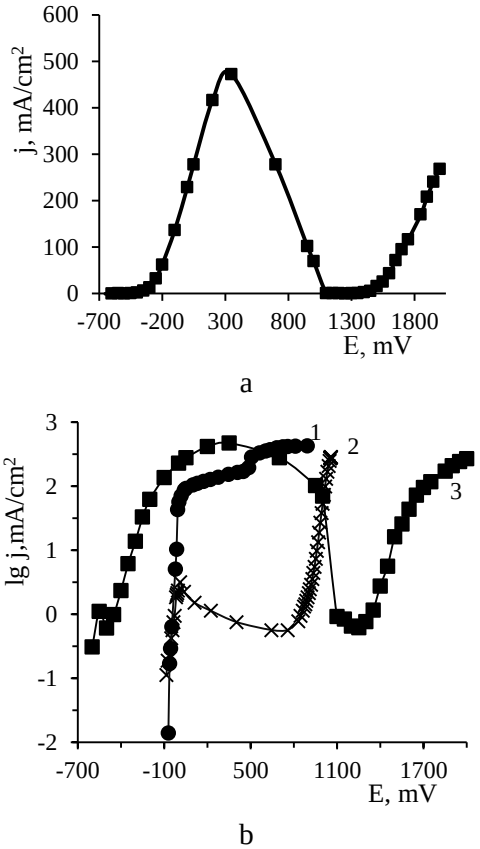

Fig.2. Anodic potentiodynamic (1 mV/s) curves of iron in (a) two-component solution and (б) in semilogarithmic coordinates. 1 – 0.05M $BaCl_2$; 2 – 0.5M $Ba(NO_3)_2$; 3 – 0.05M $BaCl_2$ + 0.5M $Ba(NO_3)_2$

Рис. 2. Анодные потенциодинамические (1 мВ/с) кривые железа в двухкомпонентном растворе (а) и в полулогарифмических координатах (б): 1 – 0,05М $BaCl_2$; 2 – 0,5М $Ba(NO_3)_2$; 3 – 0,05М $BaCl_2$ + 0,5М $Ba(NO_3)_2$

The XRD patterns of the samples obtained by means of anodic oxidation of iron in the 0.05M $BaCl_2$ + 0.5M $Ba(NO_3)_2$ solution and subsequent thermal treatment are shown in Fig. 3, and the results of XRD study as a function of heating temperature are given in Table 3. According to these data, by the DC electrolysis and subsequent drying of the precipitate at 80 °C, a dispersed material is formed, whose phase composition is a mixture of complex iron hydroxide $Fe_{0.96}O_{0.88}(OH)_{1.12}$ of goethite structure (54 wt%), witerite $BaCO_3$ (21 wt%), iron nitride Fe_4N (15 wt%), and also iron oxides – magnetite (5 wt%) and hematite (5 wt%).

The high-temperature treatment at 1200 °C of the precipitate obtained by electrolysis leads to structural ordering and the formation of barium hexaferrite $Ba_{0.87}Fe_{11.08}O_{17.15}$ (74 wt%) and barium monoferrite $BaFe_2O_4$ (17 wt%) (Fig. 3b, Table 3). In this case, the phase of iron oxide with hematite structure (5 wt%) remains unchanged in the powder composition, α-Fe phase (5 wt%) forms, the content of iron nitride significantly decreases (from 15 wt% to 1 wt%).

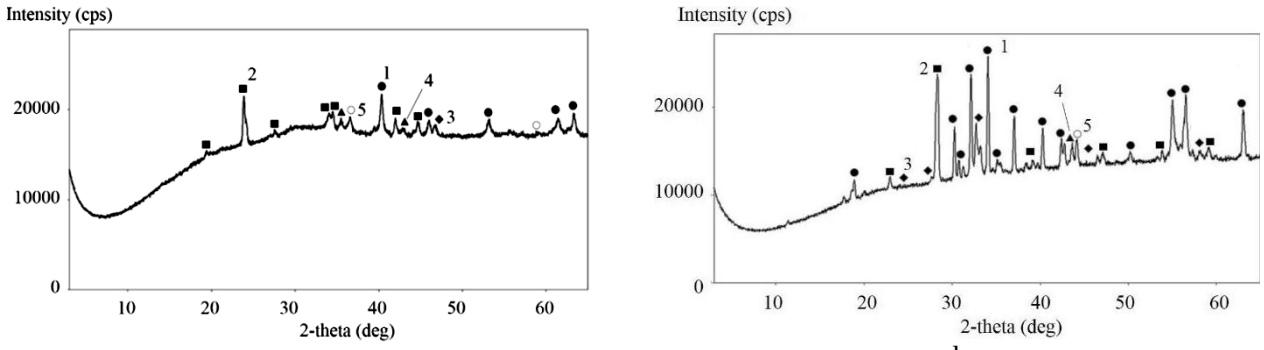

Fig. 3. XRD patterns of the samples obtained by DC electrolysis in 0.05M $BaCl_2$ + 0.5M $Ba(NO_3)_2$ solution and thermally treated at (a) 80 °C: 1 – $Fe_{0.96}O_{0.88}(OH)_{1.12}$, 2 – $BaCO_3$, 3 – Fe_4N, 4 – Fe_3O_4, 5 – α-Fe_2O_3, and (b) 1200 °C: 1 – $Ba_{0.87}Fe_{11.08}O_{17.15}$, 2 – $BaFe_2O_4$, 3 – α-Fe_2O_3, 4 – α-Fe, 5 – Fe_3N

Рис. 3. Рентгено-дифрактограммы продукта электролиза в 0,05М $BaCl_2$ + 0,5М $Ba(NO_3)_2$ и термообработанного при 80 °C: 1 – $Fe_{0.96}O_{0.88}(OH)_{1.12}$, 2 – $BaCO_3$, 3 – Fe_4N, 4 – Fe_3O_4, 5 – α-Fe_2O_3, (a) и 1200 °C (b) : 1 – $Ba_{0.87}Fe_{11.08}O_{17.15}$, 2 – $BaFe_2O_4$, 3 – α-Fe_2O_3, 4 – α-Fe, 5 – Fe_3N

Table 3

Phase composition of electrolysis products (0.05M $BaCl_2$ + 0.5M $Ba(NO_3)_2$, j=150 mA/cm^2, U=9 V, τ=60 min)

***Таблица 3*. Фазовый состав продуктов электролиза (0,05М $BaCl_2$ + 0,5М $Ba(NO_3)_2$, j=150 мА/см^2, U=9 В, τ=60 мин)**

Heating temperature, °C	Phase composition, wt.%							
	$Ba_{0.87}Fe_{11.08}O_{17.15}$	$BaFe_2O_4$	$Fe_{0.96}O_{0.88}(OH)_{1.12}$	$BaCO_3$	Fe_4N	Fe_3O_4	α-Fe_2O_3	α-Fe
80	–	–	54.0	21.0	15.0	5.0	5.0	–
1200	74.0	17.0	–	–	1.0	–	5.0	3.0

Table 4

Results of full-profile analysis of $Ba_{0.87}Fe_{11.08}O_{17.15}$ phase

***Таблица 4*. Результаты полнопрофильного анализа фазы $Ba_{0,87}Fe_{11,08}O_{17,15}$**

Size of OCD, nm (Cagliotti formula)	5990 ± 272
Magnitude of microstresses, % (Cagliotti formula)	0.14 ± 0.08
Size of OCD, nm (Halder-Wagner method)	3400 ± 23
Magnitude of microstresses, % (Halder-Wagner method)	0
Refined crystal lattice parameters	a = 5.892 Å c = 23.203 Å

Thus, DC electrolysis and subsequent high-temperature treatment (1200 °C) make it possible to obtain a dispersed product in which barium hexaferrite phase $Ba_{0.87}Fe_{11.08}O_{17.15}$ (74 wt%) dominates. The crystal lattice and microstructure parameters of barium hexaferrite phase are given in Table 4. To estimate the size of OCD, it is proposed to use the values obtained by the Halder-Wagner method, since they are less sensitive to diffraction fitting errors.

CONCLUSIONS

The anodic behavior of iron electrode in aqueous solutions of barium chloride, barium nitrate and binary electrolyte of 0.05M $BaCl_2$ + 0.5M $Ba(NO_3)_2$ was studied. The influence of electrolysis conditions (solution composition and concentration, DC value) on the intensity of anodic dissolution of technical iron (99.1%) was investigated. It was shown that the rate of anodic dissolution of iron in two-component solutions of $BaCl_2$ + $Ba(NO_3)_2$ is of the same order as in the case of dissolution in an $BaCl_2$-based electrolyte of an adequate concentration.

The possibility of synthesizing barium ferrites by anodic dissolution of technical iron (99.1%) in binary electrolyte based on barium chloride and barium nitrate and subsequent thermal treatment of the electrolysis products precipitate was shown. A dispersed system containing predominantly ferrite phases – $Ba_{0.87}Fe_{11.08}O_{17.15}$ and $BaFe_2O_4$, as well as α-Fe_2O_3, α-Fe, and Fe_3N in relatively small amounts (in total, about 11 %wt.), has been formed during DC electrolysis (ja = 150 mA/cm^2, τ = 60 min) in 0.05 M $BaCl_2$ + 0.5 M $Ba(NO_3)_2$ solution and after the high temperature treatment (1200 °C).

ЛИТЕРАТУРА

1. **Канева И.И., Костишин В.Г., Андреев В.Г., Читанов Д.Н., Николаев А.Н., Кислякова Е.И.** Получение гексаферрита бария с повышенными изотропными свойствами. *Изв. вузов. Матер. электрон. техники.* 2014. Т. 17. № 3. С.183-188. DOI: 10.17073/1609–3577–2014–3–183–188.

REFERENCES

1. **Kaneva I.I., Kostishin V.G., Andreev V.G., Chitanov D.N., Nikolaev A.N., Kislyakova E.I.** Obtaining barium hexaferrite with enhanced isotropic properties. *Izv. Vyssh. Uchebn. Zaved. Mater. Electron. Tekhniki.* 2014. V. 17. N 3. P. 183-188 (in Russian). DOI: 10.17073/1609–3577–2014–3–183–188.

2. **Pullar R.C.** Hexagonal ferrites: a review of the synthesis, properties and applications of hexaferrite ceramics. *Prog. Mater. Sci.* 2012. V. 57. N 7. P. 1191-1334. DOI: 10.1016/j.pmatsci.2012.04.001.
3. **Ozgur U., Alivov Y., Morkoc H.** Microwave Ferrites, Part 1: Fundamental Properties. *J. Mater. Sci. Mater. Electron.* 2009. V. 20. N 9. P. 789–834. DOI: 10.1007/s10854-009-9923-2.
4. **Kanagesan S., Hashim M., Jesurani S., Kalaivani T., Ismail I.** Influence of Zn–Nb on the Magnetic Properties of Barium Hexaferrite. *J. Supercond. Nov. Magn.* 2014. V. 27. N 3. P. 811-815. DOI: 10.1007/s10948-013-2357-3.
5. **Стариков А.Ю., Живулин В.Е., Прокудин А.В., Сандер Е.Е., Шерстюк Д.П., Винник Д.А.** Изучение вольтомических характеристик композитов на основе гексаферрита бария. *Вестн. ЮУрГУ. Сер. Металлургия*. 2019. Т. 19. № 1. С. 26-33. DOI: 10.14529/met190103.
6. **Topal U., Ozkan H., Sozeri H.** Synthesis and characterization of nanocrystalline $BaFe_{12}O_{19}$ obtained at 850 C by using ammonium nitrate melt. *J. Magn. Magn. Mater.* 2004. V. 284. P. 416-422. DOI: 10.1016/j.jmmm.2004.07.009.
7. **Martirosyan K., Galstyan E., Hossain S., Wang Y.-J., Litvinov D.** Barium hexaferrite nanoparticles: synthesis and magnetic properties. *Mater. Sci. Eng., B.* 2011. V. 176. N 1. P. 8-13. DOI: 10.1016/j.mseb.2010.08.005.
8. **Harris V.G., Chen Z., Chen Y., Yoon S., Sakai T., Gieler A., Yang A., He Y., Ziemer K.S., Sun N.X., Vittoria C.** Ba-hexaferrite films for next generation microwave devices (invited). *J. Appl. Phys.* 2006. V. 99. N 8. P. 08M911-1-08M911-5. DOI: 10.1063/1.2165145.
9. **Ghasemi A., Hossienpour A., Morisako A., Liu X., Ashrafizadeh A.** Investigation of the microwave absorptive behavior of doped barium ferrites. *Mater. Des.* 2008. V. 29. N 1. P.112-117. DOI: 10.1016/j.matdes.2006.11.019.
10. **Pankhurst Q.A., Connolly J., Jones S., Dobson J.** Applications of magnetic nanoparticles in biomedicine. *J. Phys. D: Appl. Phys.* 2003. V. 36. N 13. P. R167- R181. DOI: 10.1088/0022-3727/36/13/201.
11. **Veverka P., Pollert E., Zaveta K., Vasseur S., Duguet E.** Sr-hexaferrrite/maghemite composite nanoparticles – possible new mediators for magnetic hyperthermia. *J. Nannotech.* 2008. V. 19. N 21. P. 215705 (1-7). DOI: 10.1088/0957-4484/19/21/215705.
12. **Liu Y., Drew M.G.B., Liu Y., Wang J., Zhang M.** Preparation and magnetic properties of La-Mn and La-Co doped barium hexaferrites prepared via an improved co-precipitation/moltensalt method. *J. Magn. Magn. Mater.* 2010. V. 322. N 21. P. 3342-3345. DOI: 10.1016/j.jmmm.2010.06.022.
13. **Junliang L., Ping L., Xingkai Z., Dongjun P., Peng Z., Ming Z.** Synthesis and properties of single domain sphere-shaped barium hexa-ferrite nano powders via an ultrasonic-assisted co-precipitation route. *Ultrason. Sonochem.* 2015. V. 23. P. 46-52. DOI: 10.1016/j.ultsonch.2014.08.001.
14. **Yamauchi T., Tsukahara Y., Sakata T., Mori H., Chikata T., Katoh S., Wada Y.** Barium ferrite powders prepared by microwave-induced hydrothermal reaction and magnetic property. *J. Magn. Magn. Mater.* 2009. V. 321. N 1. P. 8-11. DOI: 10.1016/j.jmmm.2008.07.005.
15. **Liu Y., Drew M.G.B., Liu Y., Wang J., Zhang M.** Efficiency and purity control in the preparation of pure and/or aluminum-doped barium ferrites by hydrothermal methods using ferrous ions as reactants. *J. Magn. Magn. Mater.* 2010. V. 322. N 3. P. 366-374. DOI: 10.1016/j.jmmm.2009.09.062.

2. **Pullar R.C.** Hexagonal ferrites: a review of the synthesis, properties and applications of hexaferrite ceramics. *Prog. Mater. Sci.* 2012. V. 57. N 7. P. 1191-1334. DOI: 10.1016/j.pmatsci.2012.04.001.
3. **Ozgur U., Alivov Y., Morkoc H.** Microwave Ferrites, Part 1: Fundamental Properties. *J. Mater. Sci. Mater. Electron.* 2009. V. 20. N 9. P. 789–834. DOI: 10.1007/s10854-009-9923-2.
4. **Kanagesan S., Hashim M., Jesurani S., Kalaivani T., Ismail I.** Influence of Zn–Nb on the Magnetic Properties of Barium Hexaferrite. *J. Supercond. Nov. Magn.* 2014. V. 27. N 3. P. 811-815. DOI: 10.1007/s10948-013-2357-3.

5. **Starikov A.Yu., Zhivulin V.E., Prokudin A.V., Sander E.E., Sherstyuk D.P., Vinnik D.A.** Study of volt-ohmic characteristics of barium hexaferrite composites. *Vestn. YuUrGU. Ser. Metallurgiya*. 2019. V. 19. N 1. P. 26-33 (in Russian). DOI: 10.14529/met190103.

6. **Topal U., Ozkan H., Sozeri H.** Synthesis and characterization of nanocrystalline $BaFe_{12}O_{19}$ obtained at 850 C by using ammonium nitrate melt. *J. Magn. Magn. Mater.* 2004. V. 284. P. 416-422. DOI: 10.1016/j.jmmm.2004.07.009.
7. **Martirosyan K., Galstyan E., Hossain S., Wang Y.-J., Litvinov D.** Barium hexaferrite nanoparticles: synthesis and magnetic properties. *Mater. Sci. Eng., B.* 2011. V. 176. N 1. P. 8-13. DOI: 10.1016/j.mseb.2010.08.005.
8. **Harris V.G., Chen Z., Chen Y., Yoon S., Sakai T., Gieler A., Yang A., He Y., Ziemer K.S., Sun N.X., Vittoria C.** Ba-hexaferrite films for next generation microwave devices (invited). *J. Appl. Phys.* 2006. V. 99. N 8. P. 08M911-1-08M911-5. DOI: 10.1063/1.2165145.
9. **Ghasemi A., Hossienpour A., Morisako A., Liu X., Ashrafizadeh A.** Investigation of the microwave absorptive behavior of doped barium ferrites. *Mater. Des.* 2008. V. 29. N 1. P.112-117. DOI: 10.1016/j.matdes.2006.11.019.
10. **Pankhurst Q.A., Connolly J., Jones S., Dobson J.** Applications of magnetic nanoparticles in biomedicine. *J. Phys. D: Appl. Phys.* 2003. V. 36. N 13. P. R167- R181. DOI: 10.1088/0022-3727/36/13/201.
11. **Veverka P., Pollert E., Zaveta K., Vasseur S., Duguet E.** Sr-hexaferrrite/maghemite composite nanoparticles – possible new mediators for magnetic hyperthermia. *J. Nannotech.* 2008. V. 19. N 21. P. 215705 (1-7). DOI: 10.1088/0957-4484/19/21/215705.
12. **Liu Y., Drew M.G.B., Liu Y., Wang J., Zhang M.** Preparation and magnetic properties of La-Mn and La-Co doped barium hexaferrites prepared via an improved co-precipitation/moltensalt method. *J. Magn. Magn. Mater.* 2010. V. 322. N 21. P. 3342-3345. DOI: 10.1016/j.jmmm.2010.06.022.
13. **Junliang L., Ping L., Xingkai Z., Dongjun P., Peng Z., Ming Z.** Synthesis and properties of single domain sphere-shaped barium hexa-ferrite nano powders via an ultrasonic-assisted co-precipitation route. *Ultrason. Sonochem.* 2015. V. 23. P. 46-52. DOI: 10.1016/j.ultsonch.2014.08.001.
14. **Yamauchi T., Tsukahara Y., Sakata T., Mori H., Chikata T., Katoh S., Wada Y.** Barium ferrite powders prepared by microwave-induced hydrothermal reaction and magnetic property. *J. Magn. Magn. Mater.* 2009. V. 321. N 1. P. 8-11. DOI: 10.1016/j.jmmm.2008.07.005.
15. **Liu Y., Drew M.G.B., Liu Y., Wang J., Zhang M.** Efficiency and purity control in the preparation of pure and/or aluminum-doped barium ferrites by hydrothermal methods using ferrous ions as reactants. *J. Magn. Magn. Mater.* 2010. V. 322. N 3. P. 366-374. DOI: 10.1016/j.jmmm.2009.09.062.

16. **Paimozd E., Ghasemi A., Jafari A., Sheikh H.** Influence of acid catalysts on the structural and magnetic properties of nanocrystalline barium ferrite prepared by sol-gel method. *J. Magn. Magn. Mater.* 2008. V. 320. N 23. P. L137-L140. DOI: 10.1016/j.jmmm.2008.05.037.
17. **Meng Y.Y., He M.H., Zeng Q., Jiao D.L., Shukla S., Ramanujan R.V., Liu Z.W.** Synthesis of barium ferrite ultrafine powders by a sol-gel combustion method using glycine gels. *J. Alloys Compd.* 2014. V. 583. P. 220-225. DOI: 10.1016/j.jallcom.2013.08.156.
18. **Wang L.X., Zhang Q.T.** The effect of pH values on the formation and properties of $BaFe_{12}O_{19}$ prepared by citrate-EDTA complexing method. *J. Alloys Compd.* 2008. V. 454. N 1-2. P. 410-414. DOI: 10.1016/j.jallcom.2006.12.118.
19. **Ren P., Guan J.G., Cheng X.D.** Influence of heat treatment conditions on the structure and magnetic properties of barium ferrite $BaFe_{12}O_{19}$ hollow microspheres of low density. *Mater. Chem. Phys.* 2006 V. 98. N 1. P. 90-94. DOI: 10.1016/j.matchemphys.2005.08.070.
20. **Drofenik M., Kristl M., Žnidaršič A., Hanžel D., Lisjak D.** Hydrothermal Synthesis of Ba-Hexaferrite Nanoparticles. *J. Am. Ceram. Soc.* 2007. V. 90. N 7. P. 2057-2061. DOI: 10.1111/ j.1551-2916.2007.01740.x.
21. **Guo Y.Z., Li C.J., Wang J.N.** Fabrication and magnetic properties of nano- $BaFe_{12}O_{19}$ fibre by electrospinning. *J. Chin. Inorg. Chem.* 2009. V. 25. N 6. P. 1018-1021.
22. **Mou F., Guan J., Sun Z., Fan X., Tong G.** In situ generated dense shell-engaged Ostwald ripening: A facile controlled-preparation for BaFe12O19 hierarchical hollow fiber arrays. *J. Solid State Chem.* 2010. V. 183. N 3. P. 736-743. DOI: 10.1016/j.jssc.2010.01.016.
23. **Starowicz M., Starowicz P., Żukrowski J., Przewoźnik J., Lemański A., Kapusta C., Banaś J.** Electrochemical synthesis of magnetic iron oxide nanoparticles with controlled size. *J. Nanoparticle Res.* 2011. V. 13. N 12. P. 7167-7176. DOI: 10.1007/s11051-011-0631-5.
24. **Килимник А.Б., Острожкова Е.Ю.** Электрохимический синтез нанодисперсных порошков оксидов металлов. Тамбов: ФГБОУ ВПО «ТГТУ». 2012. 144 с.
25. **Zhang Z., Zhang Q., Xu L., Xia Y.** Preparation of nanometer γ-Fe_2O_3 by an electrochemical method in non-aqueous medium and reaction dynamics. *Synth. React. Inorg., Met.-Org., Nano-Met. Chem.* 2007. V. 37. N 1. P. 53–56. DOI: 10.1080/15533170601172468.
26. **Kalaeva S.Z., Yamanina N.S., Makarov V.M., Zaharova I.N., Shipilin A.M., Solovyova A.N., Terzi M.E.** The synthesis of nanodispersed magnetite using electrochemical method. *J. Nano-Electron. Phys.* 2014. V. 6. N 3. P. 03030-01–03030-02.
27. JCPDS PCPDFWIN: A Windows Retrieval/Display Program for Accessing the ICDD PDF-2 Database. International Centre for Diffraction Data. 1997.
28. **Halder N.C., Wagner C.N.J.** Separation of particle size and lattice strain in integral breadth measurements. *Acta Cryst.* 1966. V. 20. N 2. P. 312-313. DOI: 10.1107/S0365110X66000628.
29. **Caglioti G., Paoletti A., Ricci F.P.** Choice of Collimators for a Crystal Spectrometer for Neutron Diffraction. *Nucl. Instrum.* 1958. V. 3. N 4. P. 223-228. DOI: 10.1016/0369-643x(58)90029-x.

16. **Paimozd E., Ghasemi A., Jafari A., Sheikh H.** Influence of acid catalysts on the structural and magnetic properties of nanocrystalline barium ferrite prepared by sol-gel method. *J. Magn. Magn. Mater.* 2008. V. 320. N 23. P. L137-L140. DOI: 10.1016/j.jmmm.2008.05.037.
17. **Meng Y.Y., He M.H., Zeng Q., Jiao D.L., Shukla S., Ramanujan R.V., Liu Z.W.** Synthesis of barium ferrite ultrafine powders by a sol-gel combustion method using glycine gels. *J. Alloys Comp.* 2014. V. 583. P. 220-225. DOI: 10.1016/j.jallcom.2013.08.156.
18. **Wang L.X., Zhang Q.T.** The effect of pH values on the formation and properties of $BaFe_{12}O_{19}$ prepared by citrate-EDTA complexing method. *J. Alloys Comp.* 2008. V. 454. N 1-2. P. 410-414. DOI: 10.1016/j.jallcom.2006.12.118.
19. **Ren P., Guan J.G., Cheng X.D.** Influence of heat treatment conditions on the structure and magnetic properties of barium ferrite $BaFe_{12}O_{19}$ hollow microspheres of low density. *Mater. Chem. Phys.* 2006 V. 98. N 1. P. 90-94. DOI: 10.1016/j.matchemphys.2005.08.070.
20. **Drofenik M., Kristl M., Žnidaršič A., Hanžel D., Lisjak D.** Hydrothermal Synthesis of Ba-Hexaferrite Nanoparticles. *J. Am. Ceram. Soc.* 2007. V. 90. N 7. P. 2057-2061. DOI: 10.1111/ j.1551-2916.2007.01740.x.
21. **Guo Y.Z., Li C.J., Wang J.N.** Fabrication and magnetic properties of nano- $BaFe_{12}O_{19}$ fibre by electrospinning. *J. Chin. Inorg. Chem.* 2009. V. 25. N 6. P. 1018-1021.
22. **Mou F., Guan J., Sun Z., Fan X., Tong G.** In situ generated dense shell-engaged Ostwald ripening: A facile controlled-preparation for BaFe12O19 hierarchical hollow fiber arrays. *J. Solid State Chem.* 2010. V. 183. N 3. P. 736-743. DOI: 10.1016/j.jssc.2010.01.016.
23. **Starowicz M., Starowicz P., Żukrowski J., Przewoźnik J., Lemański A., Kapusta C., Banaś J.** Electrochemical synthesis of magnetic iron oxide nanoparticles with controlled size. *J. Nanoparticle Res.* 2011. V. 13. N 12. P. 7167-7176. DOI: 10.1007/s11051-011-0631-5.
24. **Kilimnik A.B., Ostrozhkova E.Yu.** Electrochemical synthesis of nanodispersed powders of metal oxides. Tambov: FGBOU VPO "TSTU". 2012. 144 p. (in Russian).
25. **Zhang Z., Zhang Q., Xu L., Xia Y.** Preparation of nanometer γ-Fe_2O_3 by an electrochemical method in non-aqueous medium and reaction dynamics. *Synth. React. Inorg., Met.-Org., Nano-Met. Chem.* 2007. V. 37. N 1. P. 53–56. DOI: 10.1080/15533170601172468.
26. **Kalaeva S.Z., Yamanina N.S., Makarov V.M., Zaharova I.N., Shipilin A.M., Solovyova A.N., Terzi M.E.** The synthesis of nanodispersed magnetite using electrochemical method. *J. Nano-Electron. Phys.* 2014. V. 6. N 3. P. 03030-01–03030-02.
27. JCPDS PCPDFWIN: A Windows Retrieval/Display Program for Accessing the ICDD PDF-2 Database. International Centre for Diffraction Data. 1997.
28. **Halder N.C., Wagner C.N.J.** Separation of particle size and lattice strain in integral breadth measurements. *Acta Cryst.* 1966. V. 20. N 2. P. 312-313. DOI: 10.1107/S0365110X66000628.
29. **Caglioti G., Paoletti A., Ricci F.P.** Choice of Collimators for a Crystal Spectrometer for Neutron Diffraction. *Nucl. Instrum.* 1958. V. 3. N 4. P. 223-228. DOI: 10.1016/0369-643x(58)90029-x.

Поступила в редакцию 21.09.2020
Принята к опубликованию 11.01.2021

Received 21.09.2020
Accepted 11.01.2021